Canine MR Images from 3T Active-Shield MRI System

Bo-Young Choe,[1] Chi-Bong Choi,[2] Sei-Kwon Kang,[1] Myoung-Ja Chu,[1]
Euy-Neyng Kim,[3] Hyoung-Koo Lee,[1] Tae-Suk Suh,[1]

Dept. of Biomedical Engineering[1], Kangnam St. Mary's Hospital, College of Medicine,
The Catholic University of Korea, #505 Banpo-Dong, Seocho-Gu, Seoul 137-040, Korea
Dept. of Veterinary Surgery and Radiology, College of Veterinary Medicine, Kon-Kuk University
Dept. of Nuclear Medicine[3], St. Mary's Hospital, College of Medicine, The Catholic
University of Korea, #505 Banpo-Dong, Seocho-Gu, Seoul 137-040, Korea

For veterinary imaging diagnosis, we obtained MR images of the canine brain, spine, kidney and pelvis from 3T MRI system which was equipped with the world first 3T active shield magnet.

Spin echo (SE) and Fast Spin Echo (FSE) images were obtained from the canine brain, spine, kidney and pelvis of normal and sick dogs using a homemade birdcage and transverse electromagnetic (TEM) resonators operating in quadrature and tuned to 128 MHz. In addition, we employed a homemade saddle shaped RF coil. Typical common acquisition parameters were as follows: matrix=512×512, field of view (FOV)=20cm, slice thickness=3 mm, number of excitations (NEX)=1. For T1-weighted MR images, we used TR=500 ms, TE=10 or 17.4 ms. For T2-weighted MR images, we used TR=4000 ms, TE=108 ms.

Signal to noise ratio (SNR) of 3T system was measured 2.7 times greater than that of prevalent 1.5T system. The high resolution images acquired in this study represent more than a 4-fold increase in in-plane resolution relative to conventional images obtained with a 20 cm field of view and a 5 mm slice thickness. MR images obtained from 3T system revealed numerous small venous structures throughout the image plane and provided reasonable delineation between gray and white matter.

The present results demonstrate that the MR images from 3T system could provide better diagnostic quality of resolution and sensitivity than those of 1.5T system. The elevated SNR observed in the 3T high field magnetic resonance imaging can be utilized to acquire images with a level of resolution approaching the microscopic structural level under in vivo conditions. These images represent a significant advance in our ability to examine small anatomical features with noninvasive imaging methods. Moreover, MRI technique could begin to apply for veterinary medicine in Korea.

Key Words: Magnetic resonance imaging, High field, High resolution. Veterinary medicine

Address correspondence to: Bo-Young Choe, Ph.D.
Department of Biomedical Engineering, Kangnam St. Mary's Hospital, College of Medicine, The Catholic University of Korea, #505 Banpo-Dong, Seocho-Gu, Seoul 137-040, Korea (Phone, 82-2-590-2427; Fax, 82-2-590-2425, E-mail: bychoe@cmc.cuk.ac.kr)

This study was supported by the Research Fund of Generic Industrial Technology Program(B31-973-3302-01-1-4) in Korean Ministry of Commerce, Industry and Energy.

INTRODUCTION

The first magnetic resonance imaging experiments were conducted with nuclear magnetic resonance (NMR) line scanning (1) and projection reconstruction (2) methods. While these methods established the feasibility of the magnetic resonance imaging (MRI) approach, they were characterized with relatively low spatial resolution (1,2). Nonetheless, technological achievable spatial resolution gradient design (3) and spatial encoding methods (4,5) soon permitted an increase in achievable spatial resolution, thereby greatly improving the radiological utility of MRI methods.

The need for enhanced spatial resolution in magnetic resonance arises from the desire to more precisely visualize small structures both on conventional and angiographic images. Increased spatial resolution also results in reduced susceptibility artifacts echo based MR imaging in part due to the associated increases in receiver bandwidths (6,7). In addition, enhanced spatial resolution leads to superior image interpolation required in generating MR angiograms (MRA).

Unfortunately, since magnetic resonance is an inherent technique, image resolution cannot be continuously increased without significantly compromising image quality and signal to noise (8-11). As these two characteristics progressively deteriorate, the ability to detect the structure of interest, or the visibility, also degrades. Visibility (V) can be defined as the product of the contrast-to-noise ratio (CNR) and the square root of the number of pixels (p) occupied by the object of interest. It is expressed as follows: $V = CNR \sqrt{p}$. The importance of determining appropriate spatial resolution based on visibility rather than signal-to-noise criteria alone has been addressed (12).

At 1.5T, increases in spatial resolution have often been associated with the use of specialized local surface (13) or phased array (14) radio frequency (RF) coils in order to maximize the available signal, to noise at this field strength. In addition, signal processing methods may help enhance signal to noise while preserving, as much as possible, edge definition (15-16). Using a combination of these approaches, excellent high resolution images have been obtained from the human skin (17), the extremities and cartilage (18-20), the trabecular bone (21-22), the inner ear (23-27), the eye (28-31), and the facial nerves (32-34). Increased spatial resolution has also proven valuable in MRA studies where higher resolution 3D data sets provide vessel visualization (35-36). Indeed, increased spatial resolution leads not only to the visualization of more vessels but also in the ability to differentiate progressively smaller structures. It is known for instance that vessel visibility is determined by the position of the structure of interest within the voxel grid (37). Vessels contained entirely within one voxel are thus brighter than when positioned between voxels. This is a partial volume effect that can be reduced with increased matrix size. Nonetheless, as resolution continues to increase, signal to noise to degrade to such an extent that visibility becomes compromised and the number of vessels observed no longer continues to increase. Similarly, while high resolution approaches increase functional localization in functional MRI by reducing partial volume effects, this is associated both with a significant increase in scan times and a reduction in signal to noise (38).

Despite limitations in signal to noise even with high field systems operating at 1.5T, excellent high resolution studies of the human brain have been conducted at this field strength. Using phased array detectors and an automated intensity correction algorithm, for instance, Wald et al. (39) have been able to obtain good spoiled gradient recalled volume acquisition images. In these studies, an in-plane pixel size of

0.47-0.66mm was obtained using a 0.7 mm slice thickness. Alternatively, using a fast spin echo approach were able to obtain 512×512 images with an in-plane resolution of 0.27-0.33 mm with a 1.5-3 mm slice thickness and an acquisition time of only 8.5 minutes. Similarly, Feinberg et al. (40) using the gradient-SE (GRASE) technique and partial k-space sampling, were able to obtain 2D-1024 matrix images of the human head in only 4 minutes, 20 seconds. The resulting images contained a 0.28×0.27 mm in-plan resolution from a 4 mm slice and displayed many small anatomic structures including the cochlea of the inner ear, vascular details, and the cranial nerves.

Given available field strength and total acquisition time, the previous menioned studies illustrate the potential of high resolution MRI. This conclusion can be further amplified by work performed at 4T (41-42) where high resolution modified driven equilibrium Fourier transform (MDEFT) images were obtained using a 512×512 matrix. These images had a 400-500 μm in-plane resolution from a 5 mm slice and revealed exquisite anatomical detail and gray/white matter contrast. Moreover, they display remarkable signal to noise in very high field (VHF) MRI, despite the use of standard volumetric head coils (43).

Recently, a series of 1K×1K gradient echo images with a 200 μm in-plane resolution (44-45) have been obtained from the human head at 8 Tesla (46-47) using standard transverse electromagnetic (TEM) volumetric coils (48). These images display good in-plane resolution and enhancement of the venous vasculature. In addition, they highlight the tremendous magnetic susceptibility obtained at ultra high field strengths.

MATERIALS AND METHODS

High resolution gradient recalled echo images were acquired at 128 MHz using a 3T instrument. It consists of a 3 Tesla/64 cm superconducting magnet manufactured by Oxford Magnet Technology LTD. (Witney, England) and customized gradient coil by Tesla Engineering Limited (Sussex, England). This magnet is independently ordered for the active shielded type with the weight of 11 tons. And, it is positioned within a magnetic shield constructed from annealed low carbon steel (grade 1006). Using a combination of superconductive shims located within the cryostat and resistive shims located in a specialized shim insert, the 3T magnet achieved a homogeneity of 3.78 ppm over a 40 cm diameter spherical volume established on 12-plane plot. The gradient system utilized in these studies consists of an asymmetric torque free gradient insert for whole body imaging. The gradient amplifier is capable of delivering 650V/430A on each gradient axis, and provided by MTS (MTS Systems Corporation, Horsham, PA, USA). And, spectrometer has a four channel system.

All images in this study were acquired with a Magnus 2.1 for Magnum 3T (Medinus LTD. Korea). It is equipped with Magnus Software and is able to support basic acquisition pulse sequences for fast EPI imaging, broad line imaging, 3D imaging, angiography and spectroscopy. The RF front end of the 3T system is comprised of a high power TR switch. Nonmagnetic narrow band Ga/As field effect transistor (FET) preamplifiers (Advanced Receiver Research, Burlington, CT, U.S.A) complete the front end allowing close proximity of the RF front end to the NMR coil. The quality of the receiver chain with the Magnum console was measured by examining the noise performance.

Spin echo (SE) pulse sequence was employed for T1-weighted MR images. However, for proton density and T2-weighted MR images, we used fast spin echo (FSE) with the echo train length of 8 or 16.

Radio frequency power at 128 MHz was

provided by RF amplifiers constructed specifically for this project by AMT (Herley Company, Anaheim, CA, USA). Images were acquired with a birdcage volumetric head coil and TEM head coil. The TEM coil was designed to operate in quadrature and was constructed from a group of 16 TEM struts enclosed in a copper shield.

RESULTS

T1 and T2-weighted axial and sagittal images obtained from a brain of normal dog at 3T with 256×256 matrix are displayed in Figs. 1 and 2. These images were obtained with a 4 mm slice thickness, a 12 cm FOV, using conventional SE pulse sequence. As can be seen, the contrast between white and gray matter is remarkable. And, structures of basal ganglia, internal and external capsules as well as ventricles are well discriminated.

Figure 3 shows T1 and T2-weighted axial SE images of canine brain with hydrocephaly. Note the substantial degree of increased CSF in detail. It is clearly differentiable for enlarged CSF compared with cerebral soft tissue. T1 and T2-weighted axial images of canine brain with cranial collapse are shown in Fig 4. Destructive cranial structural components are marked. T1, T2 and Gd-DTPA enhanced axial images of canine brain with extracranial tumor were shown in Fig. 5. Tumor was clearly demonstrated in GD-DTPA enhanced image (See arrow). Figure 6 shows canine brain with measles. Shape of CSF has a little bit distorted. MR angiography of normal canine brain was shown in Fig. 7. T1-weighted MR image of normal canine spine was shown in Fig. 8. Since the whole spine was not fitted in the RF coil, peripheral signal was not achieved. Kidney stone was observed in the T2-weighted MR image in Fig. 9. Note the kidney stone has dark signal (see arrow). Abnormal femoral head was observed in the T1 and T2-weighted coronal images of canine abdomen in Fig. 10. Asymmetrical morphological structure of canine pelvis was well denoted. The individual bones and joints are clearly seen.

DISCUSSION

Given the excellent technological performance of modern MRI scanners, the ability to acquire high resolution images with this modality is governed almost exclusively by available signal to noise. Thus, while excellent image scan be acquired at 1.5T, this field strength lacks the inherent signal to noise to make high resolution imaging feasible. As such, note that when conventional acquisition methods are utilized at 1.5T, it is difficult to obtain a resolution with a pixel volume much below 1 mm^3. Indeed, using a standard SE pulse sequence and a bird-cage quadrature head coil configuration with a state-of-the-art clinical scanner, images obtained with a 1 mm^3 pixel volume yielded little or no useful diagnostic information. In contrast at 3T MRI system, high resolution images (pixel volume ≤ 0.1 mm^3) can be obtained using standard imaging sequences and RF head coils without difficulty. This is the case despite the use of larger receiver bandwidths and less than fully relaxed spin excitation conditions.

T2-weighted MR image displayed in Fig. 2 was presented for appropriate reasons in that it represent the trial attempt to obtain high resolution results at 3T. In addition to provide high contrast of compatible quality in MR image, it dose reveal the potential of high field magnetic resonance imaging for increasing spatial resolution. While SNR of 3T system is increased approximately 2.7 times compared with prevalent 1.5T system, the contrast in 3T system was not proportionally increased like SNR. However, as SNR increase, the total scan time could be significantly reduced.

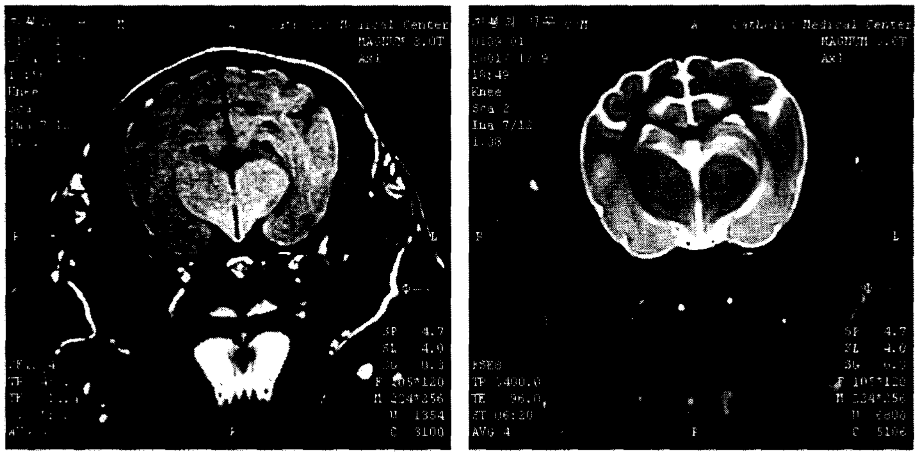

Figure 1. Typical T1-weighted axial MR images in normal canine brain using conventional spin echo pulse sequence. Parameters are TR 500ms, TE 10 ms, matrix 256×256, slice thickness 4mm, FOV 20 cm, NEX 1.

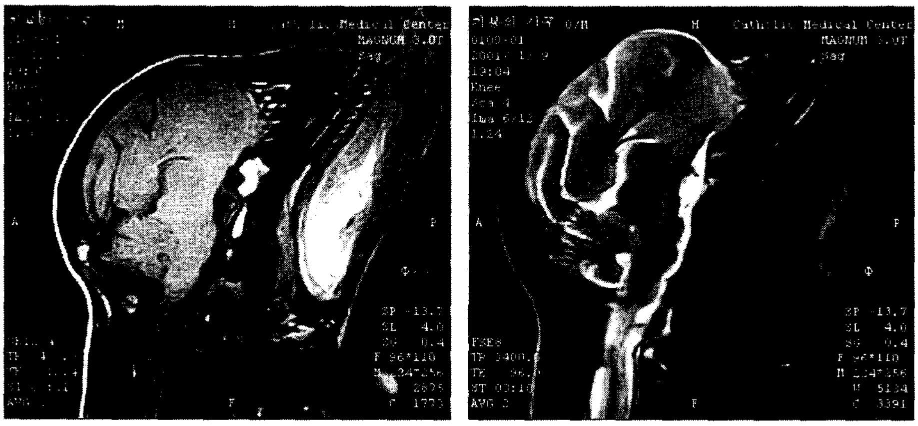

Figure 2. Typical T2-weighted axial MR images in normal canine brain using fast spin echo with ETL 8. Parameters are TR 4000ms, TF 108 ms, matrix 512×512, slice thickness 5mm, FOV 20 cm, NEX 2.

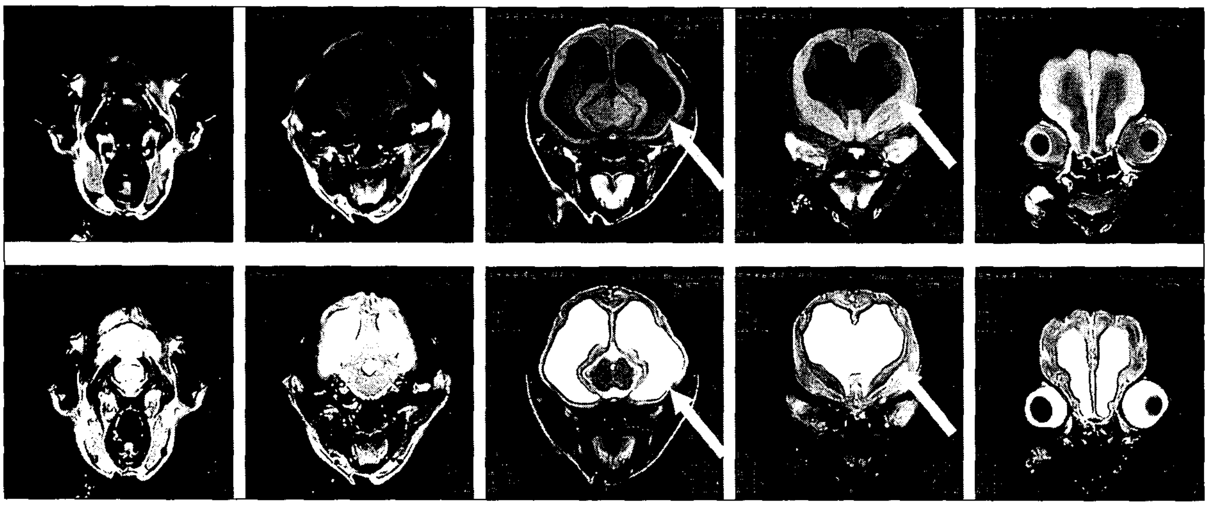

Figure 3. T1 and T2-weighted axial MR SE images of canine brain with hydrocephaly.

Figure 4. T1 and T2-weighted axial images of canine brain with cranial collapse.

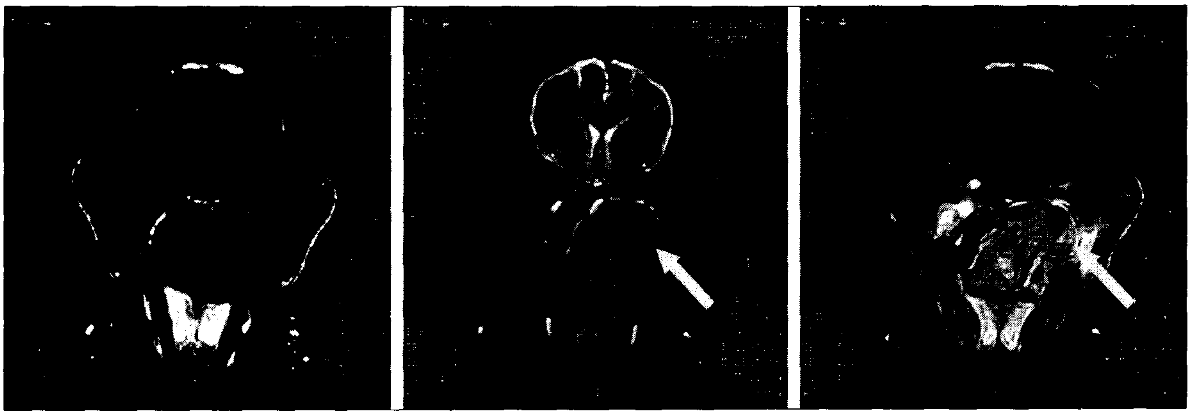

Figure 5. T1, T2 and Gd-DTPA enhanced axial images of canine brain with extracranial tumor.

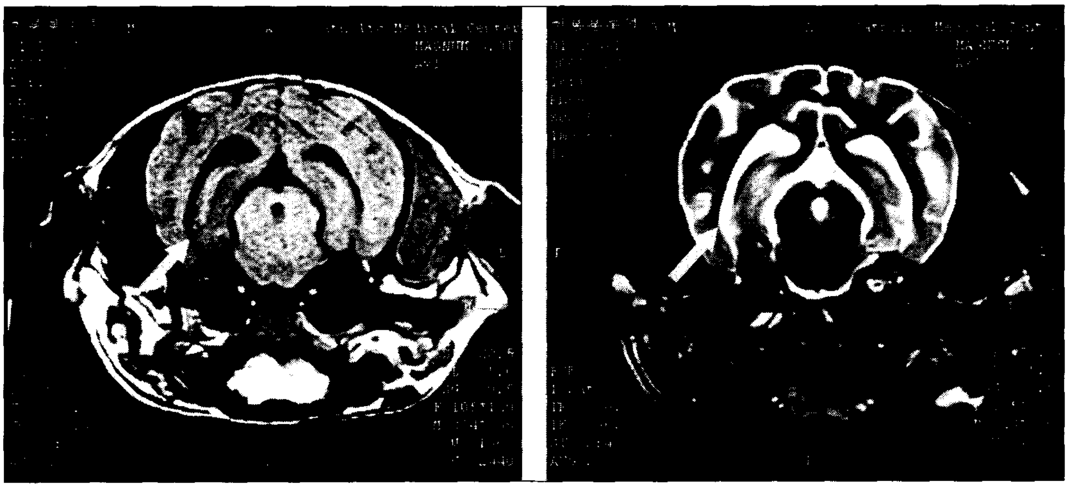

Figure 6. T1 and T2-weighted axial images of canine brain with measles.

In addition to T1-weighted MR image (Fig. 1), T2-weighted MR images were displayed in Figs. 2-4. Note the vascular detail in these images, despite the use of a standard FSE pulse sequence. Much of this vascular anatomy is venous in origin. Nonetheless, there are literally hundreds of minute vessels visible in these images. This speaks to the tremendous potential of high field MRI system in obtaining high-resolution MRA results (Fig. 8). At the same time, while the pixel resolution on these images is outstanding, it cannot be directly related to true in-plane resolution due to inherent physiological motion. Thus, it may become important to gate image

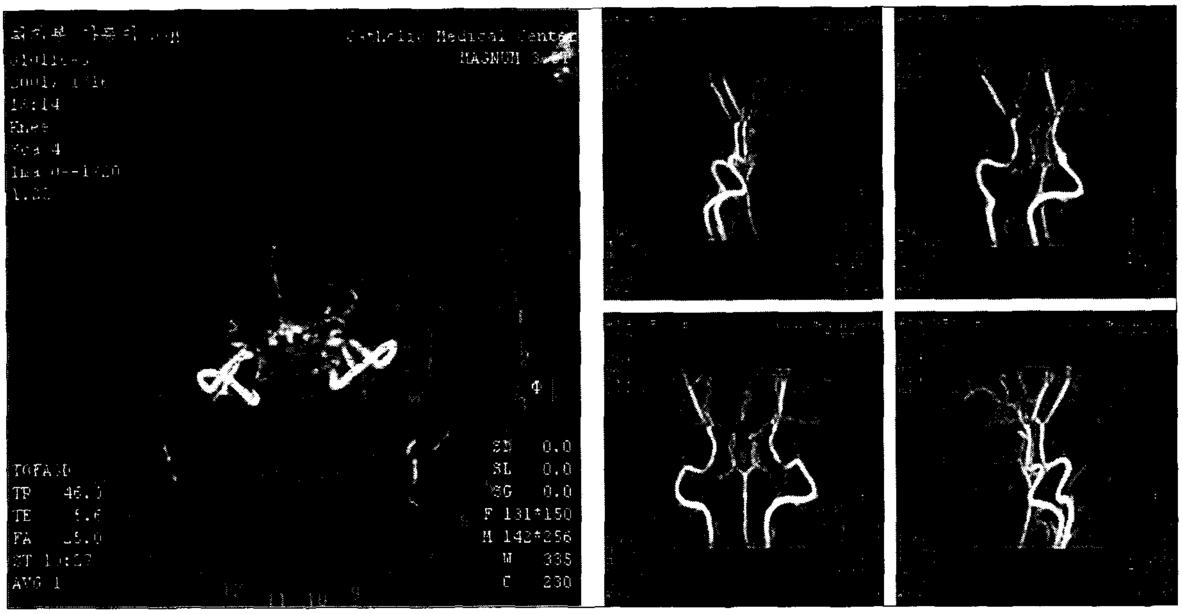

Figure 7. MR angiography of normal canine brain.

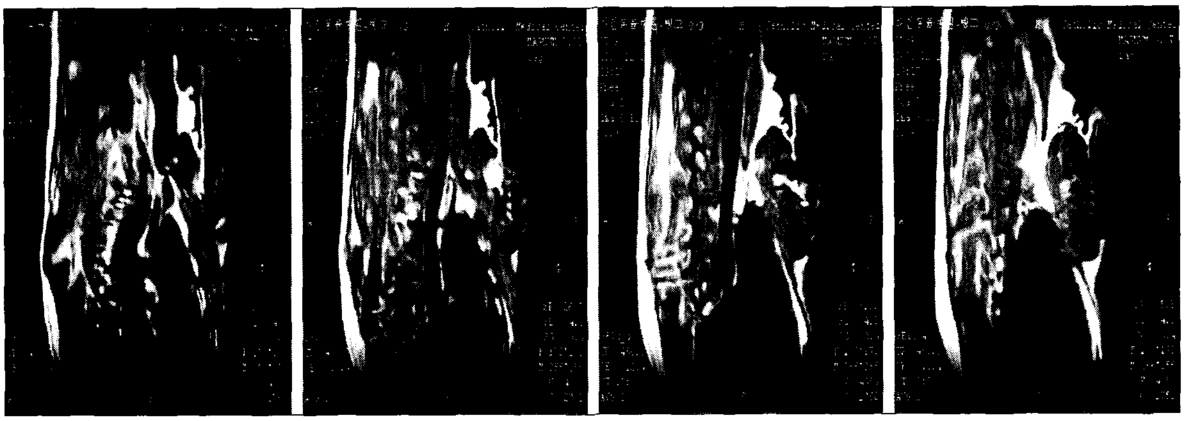

Figure 8. T1-weighted MR image of normal canine spine.

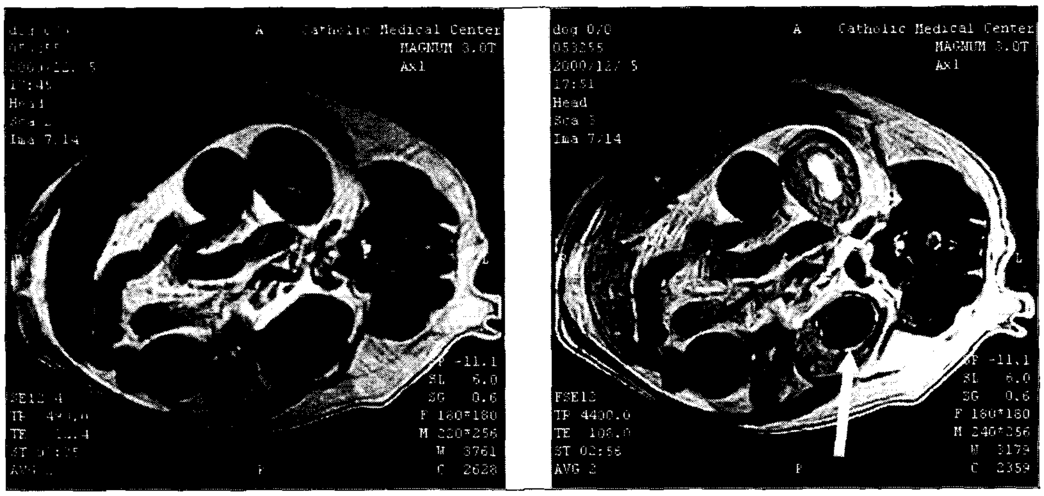

Figure 9. T2-weighted coronal MR images of canine abdomen. Kidney stone with dark signal was clearly observed (see arrow).

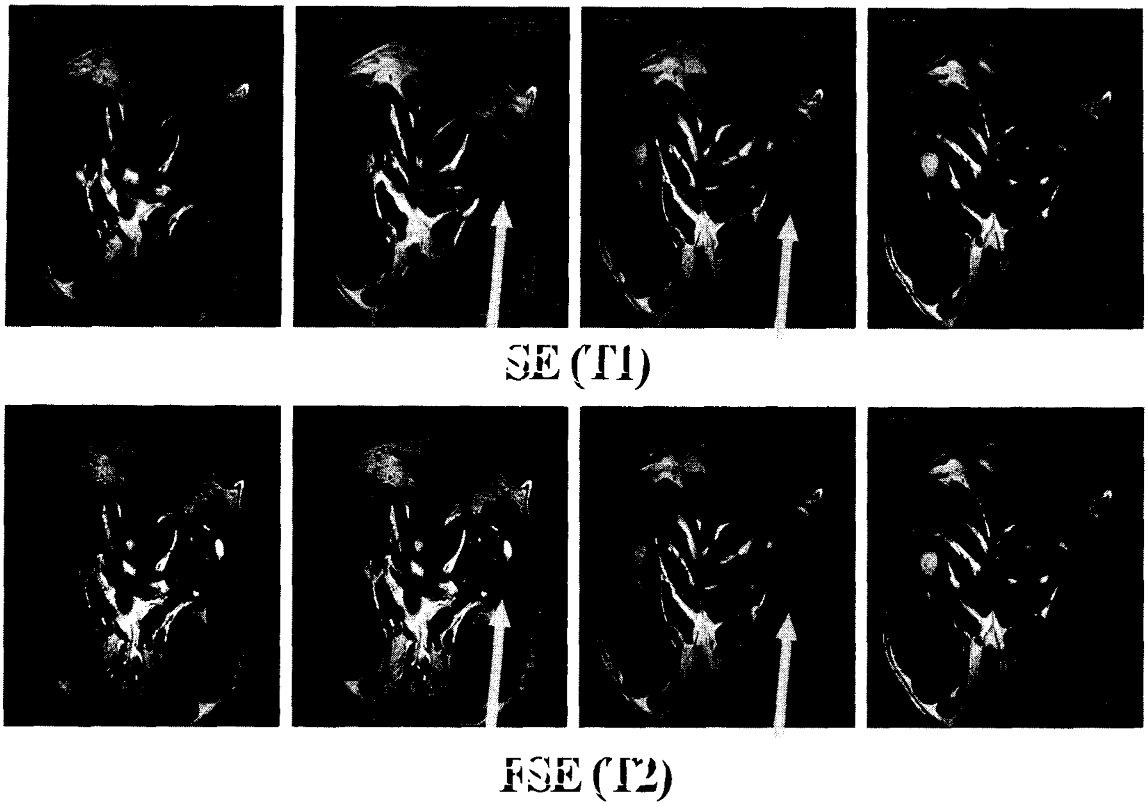

Figure 10. T2-weighted sagittal MR images of abnormal femoral head.

acquisition to cardiac or other physiological motion in order to help ensure that pixel resolution can be directly correlated to true resolution.

Nonetheless, the ability to obtain high resolution MR images will remain ultimately dictated by the Boltzmann equation. This equation determines the distribution of the spin population in the up state relative to the down state as a result of temperature and filed strength. Thus, given adequate spectrometer hardware, the only way to significantly enhance signal to noise is through a substantial increase in field strength.

The fundamental promise of high field MRI system relies on increased image resolution and decreased scanning times, both of which are critically related to intrinsic signal to noise (49). It reflects signal to noise in the absence of T1, $T2^*$, motion, flow, and scanner hardware effects. Intrinsic signal to noise, in turn must increase with field strength. It is clear from the images contained herein that the intrinsic signal to noise ratio at 3T will be phenomenal, possibly approaching a factor of 2.7 increase over a conventional 1.5T scanner. Given such performance, it is difficult to fully visualize the potential impact of high field MR image. Nonetheless, we had better insist the present trends in signal to noise and high resolution imaging continue. Finally it appears that the radiological sciences are destined to become increasingly field-strength oriented in nature.

Acknowledgment: We thank Hee-Keun Jee and all participants of CMC-Medinus 3T MRI project for their valuable assistance.

REFERENCE

1. Damadian R, Goldsmith M, Minkoff L. NMR scanning. In: NMR basic Principles and Progress. vol. 19 Diehl P, Fluck E, Kosfeld R, eds. Berlin: Springer-Verlag, 1981:1-16.

2. Lauterbur PC. Image formation by induced local interactions: example employing nuclear magnetic resonance. Nature 1973;242:190-191.
3. Mansfield P, Chapman B. Active magnetic screening of gradient coils in NMR imaging. J Magn Reson 1986;66:573-576.
4. Kumar A, Welti D, Ernst RR. NMR Fourier Zeugmatography. J Magn Reson 1975;18:69-83.
5. Edelstein WA, Hutchison JMS. Spin warp NMR imaging and application to human whole-body imaging. Phys Biol Med 1990;25:751-756.
6. Young IR, Cox IJ, Bryant D, Bydder GM. The benefits of increasing spatial resolution as a means of reducing susceptibility artifacts due to field inhomogeneities. Magn Reson Imag 1988;6:585-590.
7. Abduljalil AM, Robitaill P-ML. Macroscopic susceptibility in ultra high field MRI. J Comput Assist Tomogr 1999;23:832-841.
8. Venkatesan R, Haacke EM. Role of high resolution in magnetic resonance (MR) imaging: applications to MR angiography, intracranial T1-weighted imaging, and image interpolation. Int Imag sys Technol 1997;8:529-543.
9. Edelstein WA, Glover GH, Hardy CJ, Redington RW. The intrinsic signal-to-noise in NMR imaging. Magn Reson Med 1986;3:604-618.
10. Parker DL, Gullberg GT. Signal to noise effciency in magnetic resonance imaging. Med Phys 1990;17:250-257.
11. Hoult DI, Richards RE. The signal to noise of the nuclear magnetic resonance experiment. J Magn Reson 1976;24:71-85.
12. Constable Henkelman RM. Contrast, resolution, and detectability in MR imaging. J Comput Assist Tomogr 1991;15:297-303.
13. Ackerman JJH, Grove TH, Wong GG, Grdian DG, Radda GK. Mapping of metabolites in whole animals by 31P NMR using surface coils. Nature 1980;283:167-170.
14. Roemer PB, Edelstein WA, Hayes CE, Souza SP, Meuller OM. The NMR phased array. Magn Reson Med 1990;16:192-225.
15. Mc Veigh ER, Henkelman RM, Bronskill MJ. Noise and filtration in magnetic resonance imaging. Med Phys 1985;12:586-591.
16. Ying K, Clymer BD, Schmalbrock P. Adaptive filtering for high resolution magnetic resonance images. J Magn Reson Imag 1996;6:367-377.
17. Idy-Peretti I, Bittoun J, Alliot FA, Richard SB, Querleux BG, Cluzan RV. Lymphedematous skin and subcutis:in vivo high resolution magnetic resonance imaging evaluation. J Invest Dermatol 1998;110:782-787.
18. Potter HG, Asnin-Ernberg L, Weiland AJ, Hotchkiss RN, Peterson MGE, McCormack RR. The utility of high-resolution magnetic resonance imaging in the evaluation of the triangular fibrocartilage compex of the wrist. J Bone Joint Surg 1997;79A:1675-1684.
19. Drape JL, Peretti I, Goettmann S, Guerin-Surville H, Bittoun J. Standard and high resolution magnetic resonance imaging of glomus tumors of tose and fingertips. J Am Acad Dermatol 1996;35:550-555.
20. Waldschmidt JG, Rilling RJ, Kajdacsy-Balla AA, Boynton MD, Erickson SJ. In vitro and in vivo MR imaging of hyaline cartilage: zonal anatomy, imaging pitfalls, and pathologic conditions. Radiograph 1997; 17:1387-1402.18-20.
21. Majumdar S, Genant HK, Grampp SS, Newitt DC, Troung VHLin Jc, Mathur A. Correlation of trabecular bone structure with age, bone mineral density, and osteoporotic status: in vivo studies in the distal radius using high resolution magnetic resonance imaging. J Bone Mineral Res 1997; 12111-12118.
22. Ouyang X, Selby K, Lang P, et al High resolution magnetic resonance imaging of the calcaneous: age-related changes in trabecular structure and comparison with dual X-ray absorptiometry measurements. Calcif Tissue Int 1997;60:139-147.
23. Schmalbrock PM, Pruski J, Sun L, Rao A,

Monroe J. Phased arry RF coils for high-resolution MRI of the inner ear brain stem. J Comput Assist Tomogr 1995;19:8-14.

24. Brogan M, Chakeres DW, Schmalbrock P. High-resolution 3DFT MR imaging of the endolymphatic duct and soft tissue of the otic capsule. AJNR 1991;12:1-11.
25. Arnold B, Jager L, Grevers G. Visualization of inner ear structures by three- dimensional high resolution magnetic resonance imaging. Am J Otol 1996;17:480-485.
26. Dahm MC, Mack MG, Tykocinski M, Vogl TJ. Submillimeter imaging and reconstruction of the inner ear. Am J Otol 1997;18:S54-S56
27. Casselman JW, Kuhweide R, Deimling M, Ampe W, Dehaeme I, Meeus L. Constructive interference in steady state-3D FT MR imaging of the inner ear and cerebellopontine angle. AJNR 1993;14:47-57.
28. Ettl A, kramer J, DaxerA, Koornneef L. High -resolution magnetic resonance imaging of the normal extraocular musculature. Eye 1997;11:93-97.
29. Mashima Y, Oshitari K, Imamura Y, Momoshima S, Shiga H, Oguchi Y. Orbital high resolution magnetic resonance imaging with fast spin echo in the acute stage of Leber's hereditary optic neuropathy. J Neurol Neurosurg Psychiatry 1998;64:124-127.
30. Herrick RC, Hayman LA, Taber KH, Diaz-Marchan PJ, Kuo MD. Artifacts and pitfalls in MR imaging of the orbit: a clinical review. Radiograph 1997;17:707-724.
31. Gass A, Barker GJ, MacManus D, et al. High resolution magnetic resonance imaging of the anterior visual pathway in patients with optic neuropathies using fast spin echo and phased array coils. J Neurol Neurosurg Psychiatry 1995;58:526-529.
32. Miloro M. Halkias LE, Slone HW, Chakeres DW. Assessment of the lingual nerve in the third molar using magnetic resonance imaging. J Oral Maxillofac Surg 1997;55:134-137.
33. Dailiana T, Chakeres D, Schmalbrock P, Williams P, Aletras A. High resolution MR of the intraparotid Facial nerve and parotid duct. AJNR 1997;18:165-172.
34. McGhee RB, Chakeres DW, Schmalbrock P, Brogan MA, Negulesco JA. The extracranial facial nerve: high resolution three-dimensional Fourier transform MR imaging. AJNR 1993;14:465-472.
35. Laub GA, Kaiser WA. MR angiography with gradient motion refocusing. J Comput Assist Tomogr 1988;12:377-382.
36. Paker DL, Paker DJ, Blatter DD, Du YP, Goodrich KC. The effect of image resolution on vessel signal in high resolution magnetic resonance angiography. J Magn Reson Imag 1996;6:632-641.
37. Laub GA, Kaiser WA. MR angiography with gradient motion refocusing. J Comput Assist Tomogr 1988;12:377-382.
38. Barth M, Reichenbach JR, Vaenkatesan R, Moser E, Haacke EM. High-resolution, Multiple gradient-echo functional MRI at 1.5T. Magn Reson Imag 1999;17:321-329.
39. Wald LL, Carvajal L, Moyer SE, Nelson SJ, Grant PE, Barkovich AJ, Vigneron DB. Phased array detectors and an automated intensity-correction algorithm for high-resolution MR imaging of the human brain. Magn Reson Med 1995;34:433-439.
40. Feinberg DA, Kiefer B, Litt AW. High resolution GRASE MRI of the brain and spine: 512 and 1024 matrix imaging. J Comput Assist Tomogr 1995;19:1-7.
41. Vaughan JT, Hetherington HP, Otu JO, Pan JW, Pohost GM. High frequency volume coils for clinical NMR imaging and spectroscopy. Magn Reson Med 1994;32:206-218.
42. Pan JW, Vaughn JT, Kuzniecky RI, Pohost GM, Hetherington HP. High resolution neuroimaging at 4.1 T. Magn Reson Imag 1995;13:915-921.
43. Vaughan JT, Hetherington HP, Otu JO, Pan JW, Pohost GM. High frequency volume coils

for clinical NMR imaging and spectroscopy. Magn Reson Med 1994;32:206-218.

44. Christoforidis GA, Bourekas EC, Baujan M, Abduljlil AM, Kangarlu A, Spigos DG, Chakeres DW, Robitaille P-ML. High resolution MRI of the deep brain vascular anatomy at 8 Tesla: susceptibility-based enhancement of the venous structures. J Comput Assist Tomogr 1999;23;857-866.

45. Burgess RE, Yu Y, Christoforidis GA, Bourekas EC, Chakeres DW, Spigos D, Kangarlu A, Abduljalil AM, Robitaille P-ML. Human Leptomeningeal and cortical vascular anatomy of the cerebra cortex at 8 Tesla. J Comput Assist Tomogr 1999;23;850-856.

46. Robitaille P-ML, Abduljalil AM, Kangarlu A, et al. Human magnetic resonance imaging at 8 T. NMR Biomed 1998;11;1-3.

47. Robitaille P-ML, Warner R, Jagadeesh J, et al. Design and assembly of an 8 Tesla whole-body MR scanner. J Comput Assist Tomogr 1999;23;808-820.

48. Robitaille P-ML. Block-body and transverse electromagnetic resonators operating at 340 MHz: volume RF coils for ultra high field MRI. J Comput Assist Tomigr 1999;23:879-890.

49. Edelstein WA, Glover GH, Hardy CJ, Redington RW. The intrinsic signal to noise in NMR imaging. Magn Reson Med 1986;3:604-618.

3T 능동차폐형 자기공명영상 장비로부터 얻어진 개의 자기공명영상

가톨릭대학교 의과대학, 의공학교실,[1]
건국대학교 수의대학, 외과 및 방사선과학교실,[2]

최보영,[1] 최치봉,[2] 강세권,[1] 추명자,[1] 김의녕,[2] 이형구,[1] 서태석[1]

목적: 수의 영상진단을 위하여 3T 능동차폐형 자석을 장착한 전신용 자기공명영상장비를 이용하여 고해상도의 개 두뇌, 척추, 복부 및 골반 자기공명영상을 획득하였다.

대상 및 방법: 128 MHz의 공명주파수를 갖는 RF코일을 사용하여 정상 개 및 환축으로부터 스핀에코와 고속 스핀에코 펄스시퀀스를 적용하였다. 전형적인 펄스시퀀스의 매개변수는 512x512 matrix, 20 cm FOV, 3 mm 절편두께, 1 NEX를 사용하였다. 특히 T1 강조영상을 위하여 TR=500 ms, TE=10 혹은 17.4 ms을 사용하였으며, T2 강도영상을 위하여 TR=4000 ms, TE=108 ms을 사용하였다.

결과: 3T의 신호대잡음비는 기존 1.5T에 비하여 2.7배 정도 향상되었다. 본 연구에서 획득한 고해상도의 자기공명영상은 기존의 20cm FOV, 5mm의 절편두께와 256x256 해상도의 영상에 비하여 4배이상 증가하였다. 3T 자기공명영상은 매우 미세한 혈관 구조물을 표출하는데 도움을 주며, 또한 백질과 회질의 상당한 대조도를 제공하여 주었다.

결론: 본 연구결과에서 3T로부터 얻은 자기공명영상은 기존 1.5T 영상에서 얻은 영상에 비하여 더 높은 해상도와 민감도를 제공하여 주었다. 3T 고자장 자기공명영상에 나타난 증가된 신호대잡음비는 생체 조직단위의 영상을 획득하는데 유용하였다. 이러한 고해상도의 자기공명영상은 비침습적인 방법으로서 미세조직의 이상유무를 진단하는데 있어서 향후 더욱 임상에 도움을 주리라 예상한다. 향후 자기공명영상은 수의 진단방사선분야에 새로운 장을 열어줄 수 있으리라 기대한다.

중심단어: 자기공명영상, 고해상도, 수의 영상진단

교신저자: 최보영
가톨릭대학교 의과대학, 의공학교실, 137-040 서울시 서초구 반포동 505번지
(전화, 82-2-590-2427, 팩스, 82-2-590-2425, 전자우편, bychoe@cmc.cuk. ac.kr)